Iranian Journal of Geophysics, Vol 20 No 3, 2026, Page 129 – 151 (Research Article)
DOI: 10.30499/ijg.2025.508999.1678

3D modeling of electro-facies using a geostatistical algorithm

Reda Al Hasan[1], Mohammad Hossein Saberi[2*] and Mohammad Ali Riahi[3]

[1] M.Sc., Faculty of Chemical, Petroleum and Gas Engineering, Department of Petroleum Engineering, Semnan university, Semnan, Iran
[2] Associate Professor, Faculty of Chemical, Petroleum and Gas Engineering, Department of Petroleum Engineering, Semnan University, Semnan, Iran
[3] Professor, Institute of Geophysics, University of Tehran, Tehran, Iran

(Received: 01 March 2025, Accepted: 25 July 2025)

Abstract

Facies analysis is a critical component of reservoir characterization studies. This study employs several clustering methods to generate reservoir electro-facies (EFs) from well logs. The clustering results were then distributed using geostatistical algorithms to create a reservoir facies model within a geometrical structure interpreted from seismic data. Well logs were classified into facies using multi-resolution graph-based clustering (MRGC) and self-organizing map (SOM) methods. Once distributed spatially with geostatistical techniques, the log-derived facies supported the conditional distribution of petrophysical properties by facies. A geostatistical approach, specifically sequential indicator simulation (SIS), was used to integrate well logs and interpreted seismic data, resulting in an accurate 3D facies model. This model was generated for the depth interval spanning the Frontier (Second Wall Creek) to the Crow Mountain horizons in the Teapot Dome. The 3D facies model aids in developing the field plan and identifying potential new well locations for drilling.

Keywords: Sequential indicator simulation (SIS), electro-facies, lithofacies, MRGC, SOM

*Corresponding author: mh.saberi@semnan.ac.ir

1 Introduction

The concept of facies has been used since geologists found properties in rock units that could be used to identify coal, oil, and mineral reserves. Devised by (Gressly, 1838), the term *facies* indicates a particular collection of properties that characterize a specific sedimentary unit. In early stages, these included only geological and fossil features. A more inclusive definition was later proposed by (Selley 1976), who defined a sedimentary facies as a particular set of lithological features, geometrical characteristics, fossil abundance, sedimentary structures, and ancient flow patterns that together can characterize a specific sedimentary unit out of other assemblies. Lithology-associated facies are usually referred to as rock facies (Salley, 1986).

Clustering is an effective way to analyze data and determine facies. Facies can be determined using different clustering methods. Clustering algorithms come in two types, namely supervised and unsupervised approaches, with many instances falling under either of the two categories. In supervised clustering, the algorithm is trained on the target facies so that it can identify other instances of the target facies in the unseen data. In unsupervised clustering methods, however, the algorithm practices the classification based on the intrinsic features of the input data with no prior information on the target classes. Numerous clustering algorithms have been proposed so far, including k-means (MacQueen, 1967), spectral clustering (Fiedler, 1973), mean shift (Fukunaga & Hostetler, 1975), hierarchical clustering (Jain et al., 1999), self-organizing map (SOM) (Kohonen, 1990; Tian, 2016), and multi-resolution graph-based clustering (MRGC) (Ye, 2000), among others. They have been used in image processing (Ward et al., 2014), information retrieval (Ajil et al., 2010), statistics (Canet et al., 2010; Asante & Kreamer, 2015), and geosciences (Alizadeh et al., 2012; Hatampour et al., 2015). Recent advancements have further refined these techniques, particularly through the use of supervised methods. For instance, Bagheri and Riahi (2013) utilized support vector machines (SVMs)—a supervised algorithm that separates classes by finding optimal hyperplanes—to classify facies from seismic attributes, demonstrating their ability to manage complex, high-dimensional datasets. Similarly, Bagheri and Riahi (2015) compared SVMs with multilayer perceptrons (MLPs) and other classifiers for facies analysis using well logs, noting the slight edge of SVMs in accuracy and consistency.

Changes in the reservoir properties control hydrocarbon flows in an oil reservoir. However, the earth's anisotropy, coupled with the smoothing effect of methods like kriging, tends to mask these changes essentially, while simulation helps preserve reservoir heterogeneity. Simulation methods can be very effective in this case as they can maintain the general trend along with the data variability. Several simulation methods have been proposed for this purpose. One persistent challenge in facies classification is the overlap of classes in attribute space, which can obscure distinct geological features. To address this, Bagheri et al. (2013) introduced a dissimilarity-based classification method that utilizes 3D seismic data, reducing class overlap and enhancing the reliability of lithofacies analysis compared to conventional approaches.

Sequential indicator simulation (SIS) can model reservoir discrete properties based on the geo-cellular grid.. Applying the kriging in each cell, it forms an initial probability distribution function based on the spatial relationship between each data point (may be of unknown value) and the surrounding data points. In reservoir facies modeling, a facies index can be assigned to each cell by sampling this discrete distribution function. Accordingly, the simulated cells can be considered

known data. Hence, when geological structures are concerned, reservoir facies modeling across a field hosting a large number of closely spaced wells with suitable distribution by means of SIS leads to properly captures the trend of subsurface structures structures (Journel &Gomez-Hernandez 1993). Deutsch & A. Journel (1992) used geostatistical methods for well-log data analysis. They succeeded to develop 3D reservoir simulation methods to evaluate reservoir parameters and discover spatial relationships among well data based on the well-log data.

Deutsch & A. Journel (1992) demonstrated significant contributions in facilitating the use of well-log data in combination with seismic data for reservoir modeling. Omidvar et al. (2013) presented a 3D static model of the structural, stratigraphic, and petrophysical features of a reservoir in southern Iran. To this end, they used the well-log data acquired along 9 existing wells coupled with petrographic and core analyses and utilized kriging and sequential Gaussian simulation to propagate their model. Comparative studies indicated better accuracy of sequential Gaussian, as compared to the kriging. Bagheri and Riahi (2017) developed a new procedure for modeling or forecasting reservoir facies using seismic data with missing attributes through a dissimilarity-based classification procedure using Support Vector Machines (SVM) in dissimilarity space. Their work demonstrated promising results in high-dimensional seismic data with small training sets, where they could classify efficiently by extracting a minimal report set to train the classifier. In their study, Asadi Mehmandosti et al. (2017) presented 3D modeling of electrical facies in the Darian Formation using statistical analysis of the Reshadat Oilfield. They demonstrated the critical role of EFs modeling of carbonate reservoirs in evaluating petrophysical parameters such as porosity and permeability when petrographic data is unavailable or limited. Examining gamma-ray (GR) and density logs from 27 wells penetrating the Reshadat Oilfield in the Persian Gulf, which has limited carbonate zones, they could identify 12 EFs based on statistical clustering. They concluded that the developed 3D models were more consistent with the results of petrophysical studies on different zones of the Darian Formation and showed that EFs can play a significant role in exploring the nature of reservoirs. However, the problem remains in the large number of facies—12 EFs with different specifications—which shows the complexity of interpreting and visualizing the presented model. They did not compare their findings with the available seismic data in the study area. Abdel Fattah et al. (2018) presented a study where well seismic data was evaluated to quantify petrophysical properties of the reservoir. In this study, the oil initially in place (OIIP) and the impact of the cells dimension in reservoir modeling were investigated. Behbahani et al. (2019) undertook petrographic analysis of reservoir rock and integrated their results with tectonic studies to evaluate Madoud Reservoir, southern Persian Gulf. Using well-log data evaluation methods and 3D post-stack seismic data, they built a 3D static model of the studied reservoir based on reservoir facies analysis. Accurate integration of these data types remains critical, often requiring advanced seismic-to-well tying techniques. Amiri et al. (2020) proposed an automated approach using smooth dynamic time warping (DTW)—a method that aligns temporal sequences—to improve the correlation between synthetic seismograms and seismic traces, thereby enhancing reservoir characterization. Zare et al. (2020) developed a key technique for reservoir facies and porosity modeling in Ghar's reservoir in the Hendijan oil field, utilizing geostatistical simulation approaches that leveraged seismic data and well logs. Their research utilized multi-attribute

analyses, employing a multilayer perceptron (MLP) neural network to assess facies relationships and heterogeneity, as well as the SIS algorithm and Indicator Kriging (IKS) for facies modeling, and SGS for modeling porosity. Their work resulted in an accurate classification of facies and an estimation of porosity, while the MLP neural network successfully identified heterogeneity in the reservoir. The SGS method provided adequate three-dimensional (3D) models for porosity. Ariyan Nezhad et al. (2020) utilized the Gaussian Mixture Models (GMM) method as an unsupervised clustering technique for seismic facies analysis. This analysis was conducted on a 3D seismic dataset collected from a hydrocarbon field in southern Iran. The results demonstrate a satisfactory classification of facies using the GMM method, which aligns with the reservoir quality analyses of EFs conducted at several wells. Recent studies have advanced seismic facies analysis by employing innovative techniques, such as ANFIS and fuzzy clustering, to extract channel patterns essential for reservoir characterization (Hadiloo et al., 2017). Similarly, Mirzakhanian and Hashemi (2022) applied the adaptive Neuro-Fuzzy Inference System (ANFIS) to the fuzzy-coded well facies data to train an automatic model to predict facies from the seismic data. The results reveal that the supervised selection of attributes and fuzzy concepts is remarkable for dealing with imprecise seismic facies analysis and reservoir characterization.

According to the literature, three-dimensional reservoir models have played a crucial function in increasing the recovery, reservoir management, and drainage strategy optimization (Webber et al., 1990; Deutsch et al., 1996). For the most part, the reservoir modeling includes data collecting, building structural and stratigraphic frameworks, three-dimensional grid creation, and population of the grid cells with the petrophysical features. Most of these petrophysical features are closely related to facies attributes and facies models, which can be further integrated with the conceptual 3D geological model (Iltaf et al., 2021).The innovative techniques of seismic-well tie methodology that have also emerged over the past few years have enabled the alignment accuracy of seismic-well ties to be improved; one development uses fuzzy logic and acoustic impedance analysis combined with dynamic time warping (DTW) and has been recently introduced by Jahanjooy et al. (2025), which enhances the traditional DTW by incorporating geological characters and waveform characteristics through fuzzy feature matching. The approach focuses on matching a value assigned to a correlation metric with fuzzy impedance attributes, representing a more enhanced adjustment to calibrate the synthetic seismogram. The fuzzy attributes represent a fuzzy set that prioritizes feature-based matching instead of conventional similarity measuring. This unique and novel approach allows a new way of thinking about the problem metrics when conducting a seismic-well tie. However, it ultimately depends on the survey's intent and selecting features useful for the impedance characteristics, not just the similarities.

In the present research, we seek to determine the best reservoir facies model by taking advantage of well-logs based on two classification methods: MRGC and SOM. MRGC uses a graph-based approach to detect multi-resolution structures, allowing clusters to be identified even in data with complex or ill-defined shapes. Meanwhile, SOM relies on a self-organizing neural map that preserves the data's topological properties (spatial relationships), effectively visualizing high-dimensional data and identifying nonlinear patterns. Both methods perform better than k-means, which assumes clusters are spherical and uniform. This may not be

compatible with geophysical data's complex and nonlinear nature (such as well data), which often have irregular or overlapping distributions. However, these methods have notable limitations. The MRGC method is computationally intensive and heavily dependent on initial parameters, which can significantly restrict its practical use, especially when handling large datasets. Similarly, Self-Organizing Maps (SOM) may not effectively group similar samples, often leading to fragmented clusters that require the creation of multiple maps to align with the actual data structure accurately. To address these challenges and improve spatial facies modeling, we utilize a comprehensive facies log model in combination with sequential indicator simulation (SIS). This integrated approach aims to enhance hydrocarbon exploration by precisely identifying and characterizing the optimal rock properties in the esteemed Teapot Dome oil field, ultimately increasing the accuracy of our exploration efforts. SOM and MRGC produce accurate facies classifications based on well data (such as resistivity and gamma-ray), considering nonlinear relationships and complexities in the data. With SIS, these classifications can be used as inputs (indicators) to simulate the spatial distribution of facies between wells, ensuring that the final model reflects the geological patterns more accurately than traditional classification methods (such as k-means). The results were verified through cross-plots of some logs used for the clustering. We present photographs of the retrieved core and compare them with the identified facies. A final discussion is also presented on the results of both clustering algorithms. Despite the effectiveness of combining these methods, gaps remain related to: statistical agreement between classification and simulation, uncertainty management and computational resources, and geological validation of the model.

Overcoming these challenges requires interdisciplinary collaboration between geologists, statisticians, and petroleum engineers.

2 Geological setting

The Teapot Dome Field is situated in the Salt-Creek Anticline within the southwestern area of the Powder River Basin (PRB), located to the north of Casper in Natrona Region, Wyoming. This field is characterized by a faulted dome structure and formed a component of the Basin Margin Anticline Play within the petroleum province of the Powder River Basin (PRB) (Dolton et al., 1995, Kamran Jafri et al., 2016). The Paleozoic strata lie upon a Precambrian basement and consist of thin, alternating sequences of sandstones (resulting from dune and interdune activity), dolomites, limestone, and evaporites formed in marine environments. During the Cretaceous period, the sedimentary strata encompass a variety of formations, including fluvial sandstones, shales, as well as marine shales and sandstones.

The primary productive reservoirs within the Teapot Dome Field are the Shannon Sandstone and Second Wall-Creek Sand members of the Cody Shale, both from the Upper Cretaceous, along with the Frontier Formation. Hydrocarbons have been derived from Upper and Lower Cretaceous Formations, including the Niobrara and Steele Shale, as well as non-marine sandstone units such as the Thermopolis Shale, Muddy Sandstone, and Dakota Sandstone (Dennen et al., 2005, Kamran Jafri et al., 2016).

The Tensleep Sandstone Formation (TSF) of the Pennsylvanian era, a key producing horizon in the Teapot Dome Field, has partly originated from eolian processes. It stands as one of the multiple reservoirs contributing to oil production in Wyoming. The Tensleep Sandstone Formation (TSF) consists of marine carbonate and dolomite beds, along with porous and permeable wind-blown sandstones with

eolian cross-bedding from dune and inter-dune environments. Siliciclastic units are the predominant element of the TSF, with occasional layers of dolomite interspersed throughout (Dennen et al., 2005, Kamran Jafri et al., 2016). Refer to Figure 1 for the geological column of the Teapot Dome.

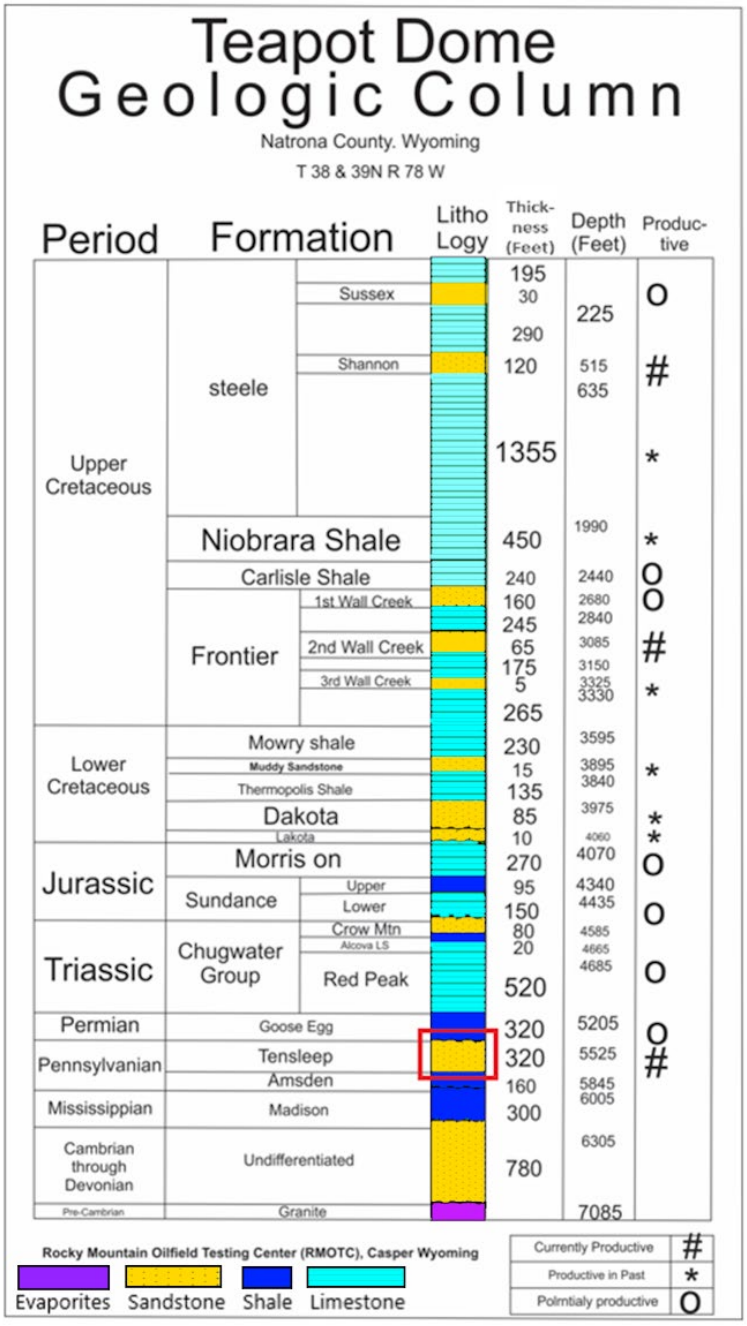

Figure 1. Geological column of Teapot Dome.

3 Studied data

Core data were available in well 48-X-28 in the depth range of 5300-5653 ft. Utilizing core photographs and descriptions, the A and B-dolomite and B-sandstone units within the Tensleep Sandstone Formation (TSF) were characterized, drawing from a previous study (Kamran Jafri et al., 2016), The image in Figure 2 displays the core from well 48-X-28, featuring the upper boundary of the B-dolomite, the lower boundary of the B-sandstone, and the C1-dolomite rock units. Considering the vast

extension of the studied area and the substantial quantity of existing wells, reliance on the poorly available core data was not reasonable and we rather directed our focus to the well-log data in the Teapot Dome Field. For this study, 45 wells were chosen due to the availability of appropriate logs for petrophysical analysis and facies modeling. The choice of wells was influenced by the presence of resistivity, GR, density, neutron, and sonic logs. The resistivity log was used to differentiate between intervals containing hydrocarbons and those containing water, identify permeable zones, and approximate the porosity. The GR log was used for shale (clay) volume (Vshale) estimation in sandstone reservoirs with uranium minerals, potassium feldspar, mica, and/or glauconite, the focus is on distinguishing between radioactive and oil shale reservoirs, assessing rock sources, evaluating potash deposits, and establishing geological correlations. The porosity was estimated using the sonic log, which relied on the measured interval transit time (Dt) of a compressive wave as it travelled through the rock formation along the central axis of the wellbore. The density log was used to identify evaporites, zones containing natural gas, and the density of hydrocarbons, thereby characterizing rock-sand reservoirs and complex rocks. Neutron logs provide a measure of porosity based on the hydrogen concentration in the formation. In shale-free formations with filled pore space containing water or oil, the neutron log is utilized to measure the porosity filled with fluid (PHIN or NPHI) (Asquith et al., 2004, Al Hasan et al., 2023).

4 Methods

In the Geolog software (AspenTech TM), SOM and MRGC were utilized for clustering well-log data. To enhance our comprehension of the distinct functionalities of both methods, we provide the pseudo-code for each in Tables 1 and 2. These tables meticulously outline the algorithms we have employed, offering a clear insight into their operational frameworks.

Learning Rate (α): Controls the update size (usually starting at 0.9 and decreasing to 0.01). Neighborhood Radius (σ): Starts large (similar to the network radius) and decreases over time.

4-1 Indicator Kriging

The indicator kriging refers to the kriging of the indicator variable. An indicator variable is a numeric representation of a categorical variable with two potential outcomes: the presence or absence of a categorical symbol. Binary facies, such as sandstone/shale or limestone/dolomite, can be readily classified using an indicator variable. In cases where facies have three or more codes, they are addressed within a specific model. In this model, a specific facies is represented by its presence, while

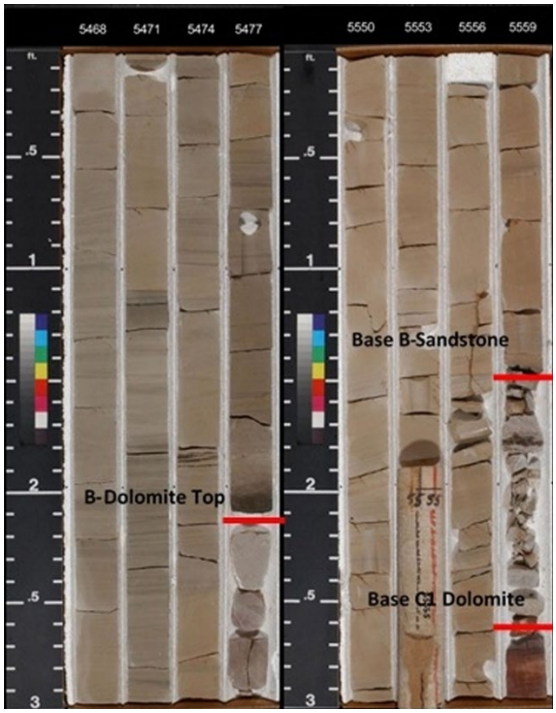

Figure 2. Core box photograph from well 48-X-28 showing the top of B-dolomite, and the base of B-sandstone and C1-dolomite rock units (Kamran Jafri et al., 2016).

Table 1. The Algorithm of Self-Organizing Map (Kohonen, 1990).

Input: Data X, Network Size *nm*, Number of Iterations T
Output: Network Weights **W**
1: Initialize the weights $\mathbf{W}_i$ randomly or using PCA.
2: **for** $t = 1$ to T **do**
3: Select a random sample $\mathbf{x} \in \mathbf{X}$.
4: Compute the Best Matching Unit (BMU):

$$BMU = arg\min_i ||\mathbf{x} - \mathbf{W}_i||_2 .$$

5: Update the weights of all nodes:
6: **for** each node j in the network **do**
7: Compute the topological distance between j and the BMU.
8: Compute the learning rate $\alpha(t)$ and the neighborhood function $h_{BMU,j}(t)$.
9: Update the weight:

$$\mathbf{W}j \leftarrow \mathbf{W}j + \alpha(t) \cdot hBMU, j(t) \cdot (\mathbf{x} - \mathbf{W}j)$$

10: **end for**
11: **end for**
13: Repeat until convergence.

Table 2. The Algorithm of MRGC method (Ye, 2000).

Input: Data **X**, Number of resolution levels K, similarity coefficient σ
Output: Clustering labels (Labels)
1: **for** each resolution level $k = 1$ to K **do**
2: Create a similarity matrix **W** using a Gaussian similarity function:

$$W_{ij} = exp\left(-\frac{\|\mathbf{x}_i - \mathbf{x}_j\|^2}{2\sigma^2{}_k}\right)$$

3: Compute A Degree Matrix **D** :

$$\mathrm{D}_{ij} = \sum_{\mathrm{j}=1}^{n} \mathrm{W}_{\mathrm{ij}}, \qquad \mathrm{D}_{ij} = 0 \text{ for } i \neq j$$

4: Compute the Laplacian Matrix **L**:

$$\boldsymbol{L} = \boldsymbol{D} - \boldsymbol{W}$$

5: Compute the eigenvectors for **L**.
6: Apply the K-Means algorithm to the eigenvectors to obtain the initial clustering.
7: **end for**.
8: Combine the clustering results from all resolutions using majority voting or contextual evaluation.
9: Perform the final re-clustering based on the optimal resolution.

the absence of that facies code is indicated by the combination of all other codes. This is repeated for all facies. Each indicator value's estimated value represents its likelihood of occurrence. The likelihood of each facies is determined using a linear model that considers its overall ratio and neighboring data (Ma & Zhang, 2019).

4-2 Sequential indicator simulation (SIS)

Sequential Indicator Simulation (SIS) represents a stochastic simulation approach designed for an indicator variable. It operates as the stochastic simulation method (sequential Gaussian simulation) for continuous variables.

The approach involves simulating the facies code by graphing its local probability distribution (Deutsch & Journel, 1992). Local probability distributions are produced with consideration for categorical codes that are present in wells or have already been simulated. SIS is an extension of Indicator kriging method in which local PDF of each facies is computed at grid nodes. PDFs are randomly sampled to obtain the geostatistical realisation (most probable facies). A random walking path is used to select the sequence of grid nodes where to compute the property (Ma & Zhang, 2019). Table 3 shows the main differences between SIS and SGS. Figure 3 shows the workflow of this study.

Table 3. Essential Distinctions Between SIS and SGS.

Criterion	Sequential Indicator Simulation (SIS)	Sequential Gaussian Simulation (SGS)
Data Type	**Categorical variables** (e.g., facies - sand/shale/carbonate).	**Continuous variables** (e.g., porosity, permeability).
Statistical Assumptions	No specific distribution required.	Assumes **Gaussian distribution** (or transformable to Gaussian).
Coding Method	Uses **indicator coding** (0 or 1) for each category.	Processes continuous values directly (or after Gaussian transform).
Spatial Structure	Uses **indicator variogram** for each category.	Uses a **single variogram** for the continuous variable.
Boundary Handling	Preserves **sharp boundaries** between categories.	May produce **smoothed transitions** between values.
Geological Complexity	Suitable for **highly heterogeneous** environments (e.g., fluvial channels).	Best for **relatively homogeneous** distributions.
Outputs	Categorical maps (facies distribution).	Continuous value maps (e.g., porosity distribution).
Common Applications	Facies modeling, geological unit identification.	Modeling petrophysical properties (e.g., permeability).
Noise Resistance	Better with **heterogeneous/noisy data**.	Sensitive to outliers if not properly transformed.
Statistical Flexibility	No complex data transformations needed.	Requires **normal score transformation** for non-Gaussian data.

4-2-1 Role of Variograms in SIS

Variograms define the spatial correlation structure for each category. Directional variograms (major/minor ranges, azimuth) ensure spatial patterns align with geological trends.

For a category k, define the indicator function:

$$I_x(x) = \begin{cases} 1 & if\ location\ x\ belongs\ to\ category\ k, \\ 0 & otherwise \end{cases} \quad (1)$$

For each category k, compute the experimental variogram and fit a theoretical model (e.g., spherical, exponential):

$$\gamma_k(h) = C_{0k} + C_k\,.Model\left(\frac{h}{a_k}\right) \quad (2)$$

where:

- C_{0k}: Nugget effect (microscale variability),
- C_k: Partial sill (category-specific variance),
- a_k: Range parameter (distance of spatial correlation).

For directional continuity, use a transformed lag distance h_{eff}:

$$h_{eff} = \sqrt{\sqrt{\left(\frac{h_x\cos\theta + h_y\sin\theta}{a_{major,k}}\right)^2 + \left(\frac{-h_x\sin\theta + h_y\cos\theta}{a_{minor,k}}\right)^2}} \quad (3)$$

where:

- $a_{major,k}$, $a_{minor,k}$: Major/minor ranges for category k,
- θ : Azimuth (angle of the major direction).

Building a reservoir model begins with collecting basic data from wells, including geophysical well logs (such as Gr and LLD), and then analyzing rock samples from cores. This data undergoes a rigorous quality control process and is cleaned of artifacts or anomalies to ensure reliability. Intelligent clustering techniques are used to analyze the data further, such as the SOM algorithm, which transforms complex data into two-dimensional maps, and the MRGC method, which reveals geological patterns at multiple resolutions. After comparing the results of these two methods, the most accurate is selected to create what are known as "EFs," a digital representation of the rock units in the wells. These facies are adjusted to fit the three-dimensional model through a scale-up

process and then integrated with the underlying geological structures (such as strata and faults) constructed using engineering data. The SIS algorithm simulates the facies distribution between wells to spatialize the model. To enhance the model's accuracy, the interpreted seismic data are combined and matched with well data through a precise correlation process, then converted from seismic time to depth to match the well model. Finally, all these elements are integrated into a three-dimensional model depicting the distribution of lithofacies in the reservoir. Figure 3 shows the workflow of this study.

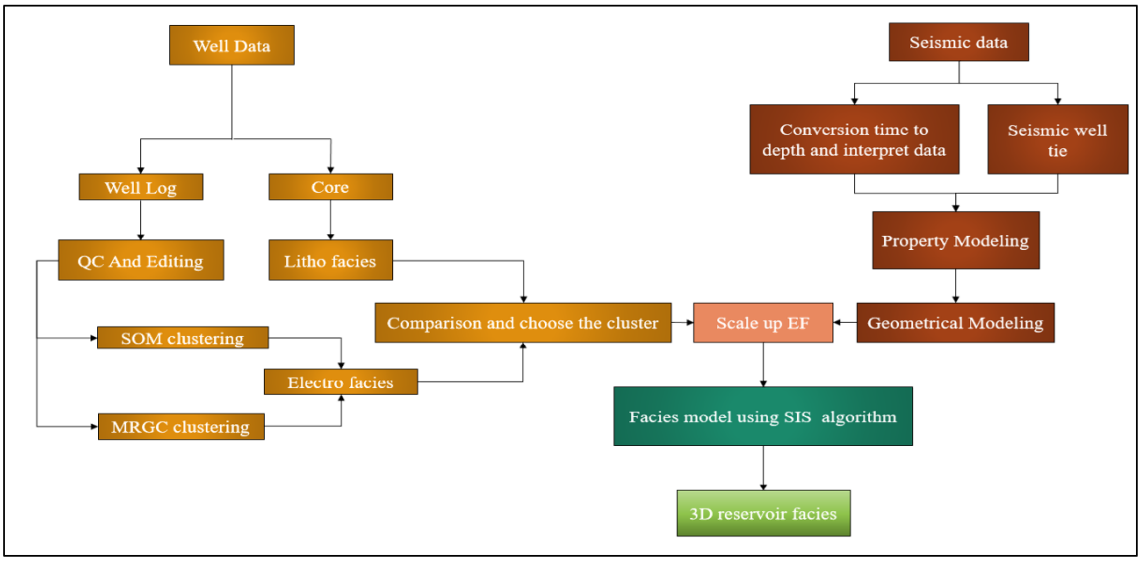

Figure 3. The workflow of this study.

5 Results and discussion

Initially, depth matching was conducted using GR log values, and any essential adjustments were applied. To validate the data, facies clustering was conducted by the Geolog Facimage™, where a well (48-X-28) with good-quality data was selected and the acquired logs at the selected wells were used to train the algorithm. 48-X-28Results indicated suitable distribution of the log data, and this confirmed the appropriateness of the log selection, so that we could proceed to evaluation process. Through the cross-plot of these logs (see Al Hasan et al., 2023). On this figure, the colors indicate data frequency. In fact, this figure indicates that some well-log data exhibit similar trends and good correlation to one another. This is reflected by the frequency of data points within the GR and DT ranges of 60-120 API and 200-350 US/M, respectively. This reflects the association of high reservoir quality with low GR values.

5-1 SOM clustering results

Table 4 exhibits the outcomes of the SOM clustering technique at the utilized wells. Next, comparable EFs were consolidated to prevent overgrowth of the EFs . Upon analyzing the clustering results, it was observed that EF1 and EF2 exhibit high statistical and physical similarities, justifying their representation as a single EF; the same was seen for EF3 and EF5. This reduced the final number of the EFs to 7 mains EFs. The cross-plot clearly indicated that EF1 and EF7 correspond to the highest and lowest reservoir qualities, respectively. EF2 to EF6 exhibited relatively similar values, making the corresponding zone of medium reservoir quality. Finally, the nearest-neighbor method was utilized to generalize the EFs model to the entire length of the well (see Al Hasan et al., 2023).

Table 4. Results of the SOM clustering method for the studied wells (Al Hasan et al., 2023).

Facies	Weight	GR	GRR	LLD	MSFL	NPHI	RHOB	DT
1	2102	112.6	112.6	6.73	5.41	0.31	2446.56	292.02
2	986	107.66	107.66	8.46	7.14	0.27	2498.03	274.07
3	642	99.6	99.6	13.31	11.73	0.21	2576.58	244.24
4	1636	99.39	99.39	8.15	6.71	0.29	2483.24	292.6
5	342	90.03	90.03	12.71	10.41	0.23	2526.39	269.09
6	860	78.2	78.2	25.63	20.38	0.16	2600.23	234.9
7	1300	84.85	84.85	10.15	8.4	0.27	2506.88	292.29
8	871	71.32	71.32	19.91	15.25	0.2	2539.06	263.82
9	1295	58.16	58.16	47.52	32.71	0.13	2608.41	228.93

5-2 MRGC results

Unsupervised MRGC clustering method can be used to group different areas, categories, or facies of identical characteristics into a dataset. In unsupervised clustering methods (*e.g.*, SOM), the number of final classes is predetermined, while supervised methods (*e.g.*, MRGC) set the number of final categories considering the dimensions within the corresponding space and the density of the data distribution. After categorizing, the used well-log data can be cross-plotted to come up with clearly separated data points for each class of data (*i.e.*, shown in different colors). After setting the list of EFs, the count of EFs and distribution of each log for each EFs can be investigated. That is, the allocation of samples to each EFs and the calculation of average values for each well-log within those EFs facilitated the derivation of optimal models for 10, 14, 18, 20, and 23 EFs. Considering the literature and geological setting of the study area, the best combination of EFs was obtained with a 10-EFs model. Table 5 displays the outcomes of the MRGC method applied to the utilized wells.

Table 5. Results of the MRGC method for the studied wells (Al Hasan et al., 2023).

Facies	Weight	GR	GRR	LLD	MSFL	NPHI	RHOB	DT
1	404	26.29	26.29	560.95	248.75	0.05	2816.93	191.49
2	382	28.32	28.32	187.33	49.83	0.06	2534.12	202.22
3	1014	57.35	57.35	15.78	13.77	0.18	2455.48	270.87
4	672	72.81	72.81	31.04	32.78	0.1	2665.26	217.67
5	800	100.7	100.7	23.66	22.49	0.16	2696.15	202.82
6	950	94.82	94.82	8.48	8.08	0.21	2541.57	260.87
7	360	118.49	118.49	3.74	2.08	0.38	2252.92	295.22
8	2512	91.52	91.52	8.35	6.97	0.3	2521.24	305.81
9	2255	122.38	122.38	7.14	6.48	0.3	2488.05	288.97
10	685	87.22	87.22	5.07	2.3	0.34	2281.75	263.87

Similarly to the SOM method, it is important to merge EFs with comparable properties in order to avoid overgrowth of the EFs . The final number of EFs was reduced to 7 after this adjustment. The cross-plot indicates that EF1 and EF2 represent the best reservoir quality while EF6 and EF7 represent the worst. EF3 to EF5 exhibit more-or-less close properties associated with moderate reservoir qual-

ity. The nearest-neighbor method was finally applied to propagate the EFs modeling along the entire well. The identified EFs on petrophysical logs can be observed and compared (see Al Hasan et al., 2023).

5-3 Prioritizing EFs Logs According to Reservoir Quality

The quality of the reservoir is determined by porosity, permeability, shale volume, and hydrocarbon content. Hence, any geological factor that enhances these parameters within a reservoir contributes to improved reservoir quality. An influencing factor may be either physical or chemical. The generated EFs logs were analyzed and ranked based on reservoir quality. In this study, the reservoir quality was assessed considering analyzed logs. EFs logs, were interpreted using box-plot diagrams. Figure 4 illustrates the variation of GR and DT logs within distinct EFs identified through the use of SOM and MRGC methods. Certainly, lower GR readings and/or higher DT readings correspond to improved reservoir quality. As depicted in Figure 4a, EF1 and EF2 represent the highest reservoir quality, denoted by their low GR readings (indicative of minimal shale volume), whereas EF7 signifies the lowest reservoir quality characterized by its elevated GR readings. Figure 4b illustrates that EF1 represents the best reservoir quality, while EF7 represents the worst. Figure 4c displays DT values spanning from 200 to 300 microseconds per meter, while Figure 4d showcases corresponding DT readings within the range of 150 to 300 microseconds per meter. Establishing a connection between EFs and petrophysical properties is crucial for quantitatively assessing geological results. Figure 5 illustrates the correlation between the gamma ray (Gr) log and the neutron porosity (NPHI) log. This relationship directly indicates porosity within the rock formation, allowing for a more detailed understanding of the subsurface characteristics. By analyzing these logs together, we can gain valuable insights into the reservoir quality, ultimately enhancing the evaluation of hydrocarbon potential in the area.

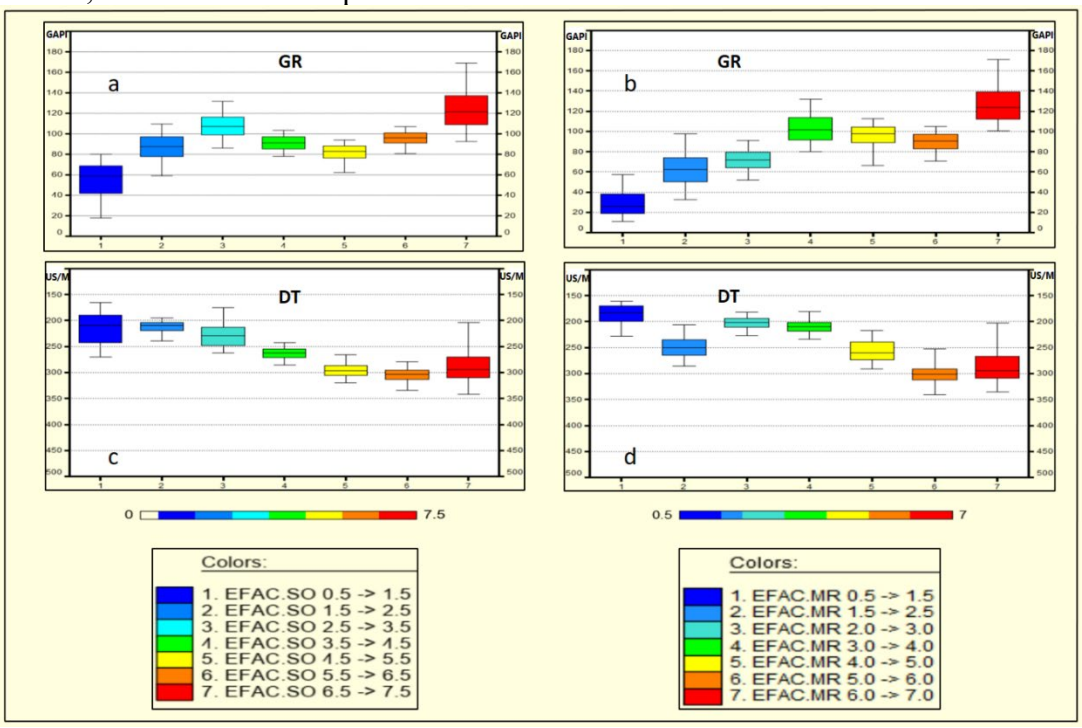

Figure 4. (a, b) Boxplots of GR log for the EFs obtained from the SOM and MRGC algorithms, and (c, d) boxplots of DT log for the EFs obtained from the SOM and MRGC algorithms (Al Hasan et al., 2023).

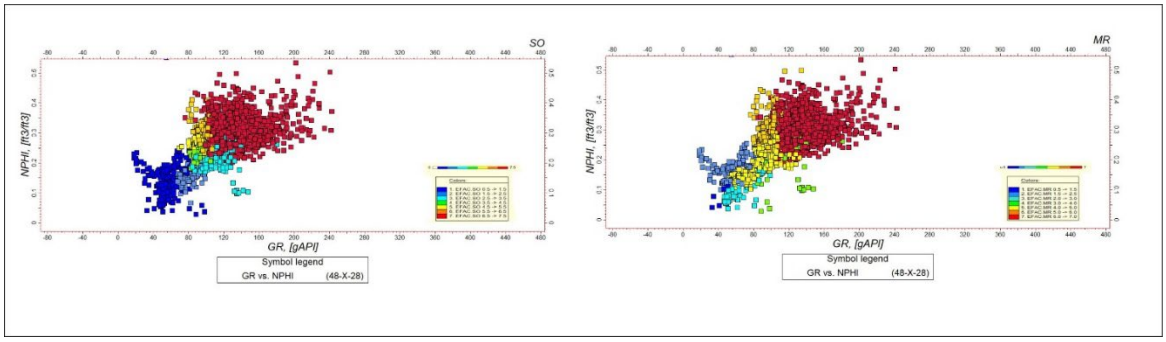

Figure 5. The correlation between the gamma ray (Gr) log and the neutron porosity (NPHI) log, labeled with EFs. Left: sourced from SOM, Right: sourced from MRGC.

The analysis indicates that both methods identify EF1 and EF2 as associated with the highest reservoir quality. In contrast, EF6 and EF7 indicate the lowest reservoir quality using the SOM and MRGC approaches. In industrial applications, an attempt is usually made to classify facies under good and bad facies. Such a general classification would provide an easy-to-understand reference for drilling (see Al Hasan et al., 2023). Figure 6 presents some well logs from the well (48x-28) coupled with the results of MRGC and SOM versus depth. The figure indicates better accuracy of the MRGC rather than SOM. It's interesting to note that the core data was collected from the specified depth range of 5300-5653 feet, and Figure 7 showcases photographic images of the core samples. Figure 7-a corresponds to EF1 with the highest porosity coupled with lowest GR; this EF was found to be widely distributed in different depths (*i.e.*, 5445-4765 ft). Figure 7-b exhibits EF2 with GR readings close to EF1 and maximum abundance in the depth ranges of 2855-2905 and 4330-4370 ft. Figure 7-c corresponds to EF1 from SOM and EF3 from MRGC with moderate reservoir quality in the depth ranges of 500-535 and 5586-5590 ft. Figure 7-d demonstrates EF4 with poorer reservoir quality than EF3; this EF was identified in the depth ranges of 4290-4305, 4690-5115, and 5265-5300 ft. Figure 7-e refers to EF5 with medium-to-poor reservoir quality based on porosity and GR values; this EF was identified in the depth ranges of 2485-2670, 2910-3050, and 3950-4275 ft. Figure 7-f represents EF6, demonstrating poor reservoir quality within the depth intervals of 535-1330, 2000-2075, 3859-3930, and 4290-4330 feet. Finally, figure 7-g depicts EF7 with very poor reservoir properties in depth ranges of 1550-2470, 2715-2850, 3055-3845, and 4585-4600 ft. Upon comparing the outcomes of the two algorithms using well logs, we observed that MRGC demonstrated superior accuracy compared to SOM.

6 Geological modelling

Reservoir facies models can be used in different stages of oil exploration. The modeling process consisted of three steps: data loading, structural modeling, and property modeling. In the initial phase, well data is meticulously collected and loaded, offering reliable spatial information regarding the reservoir's characteristics and distribution. This data serves as the backbone of the modeling process. The subsequent phase involves structural modeling, which is executed using the gathered data to depict the geological framework accurately. This begins with defining an initial model, focusing on critical horizons such as the Second Wall-Creek Sand and Crow Mountain horizons, which are identified as the main reservoir zones. During this phase, various geological features, including interpreted fault models, are constructed to understand the complexity of the reservoir. To enhance

the model's accuracy, interpreted fault models are thoroughly presented. These models show the intricate relationships between different geological layers and the potential impact of these faults on fluid flow within the reservoir. Figure (8) illustrates these interpreted faults, providing a visual representation that aids in understanding the structural complexities of the reservoir.

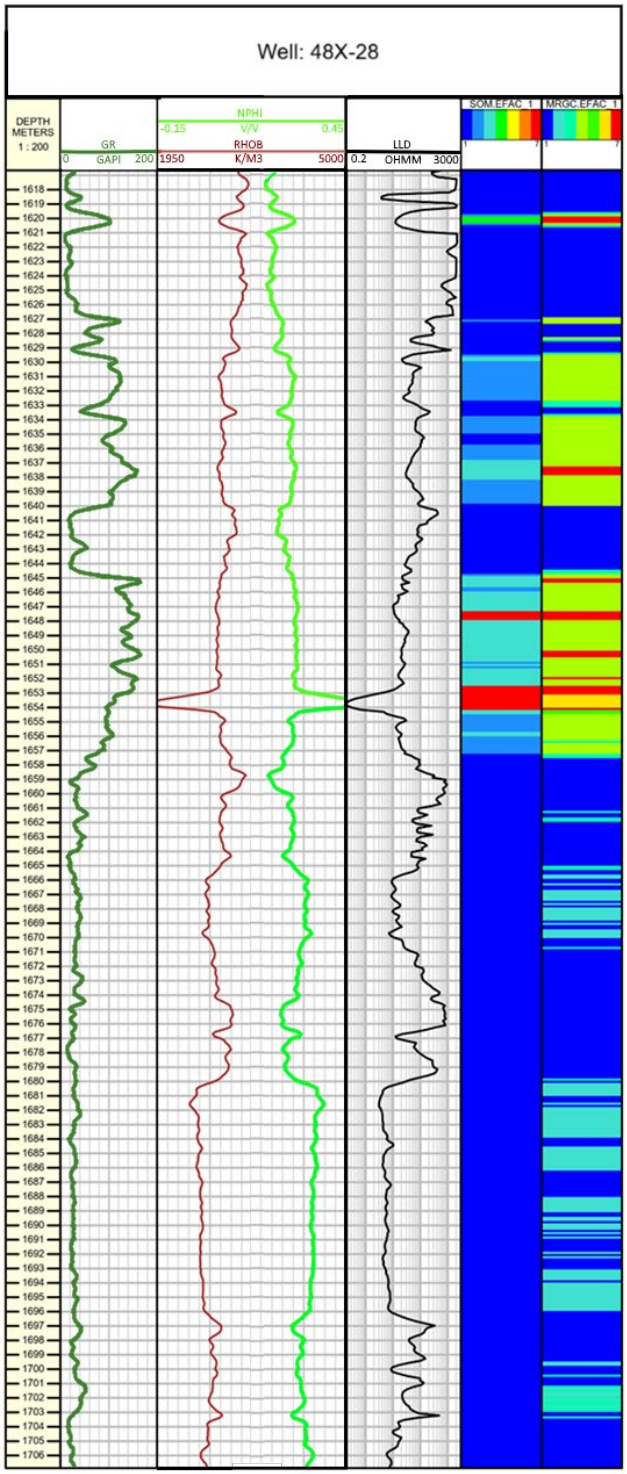

Figure 6. Comparing the results of EFs modeling based on MRGC and SOM with the petrophysical well-logs for well 48x-28.

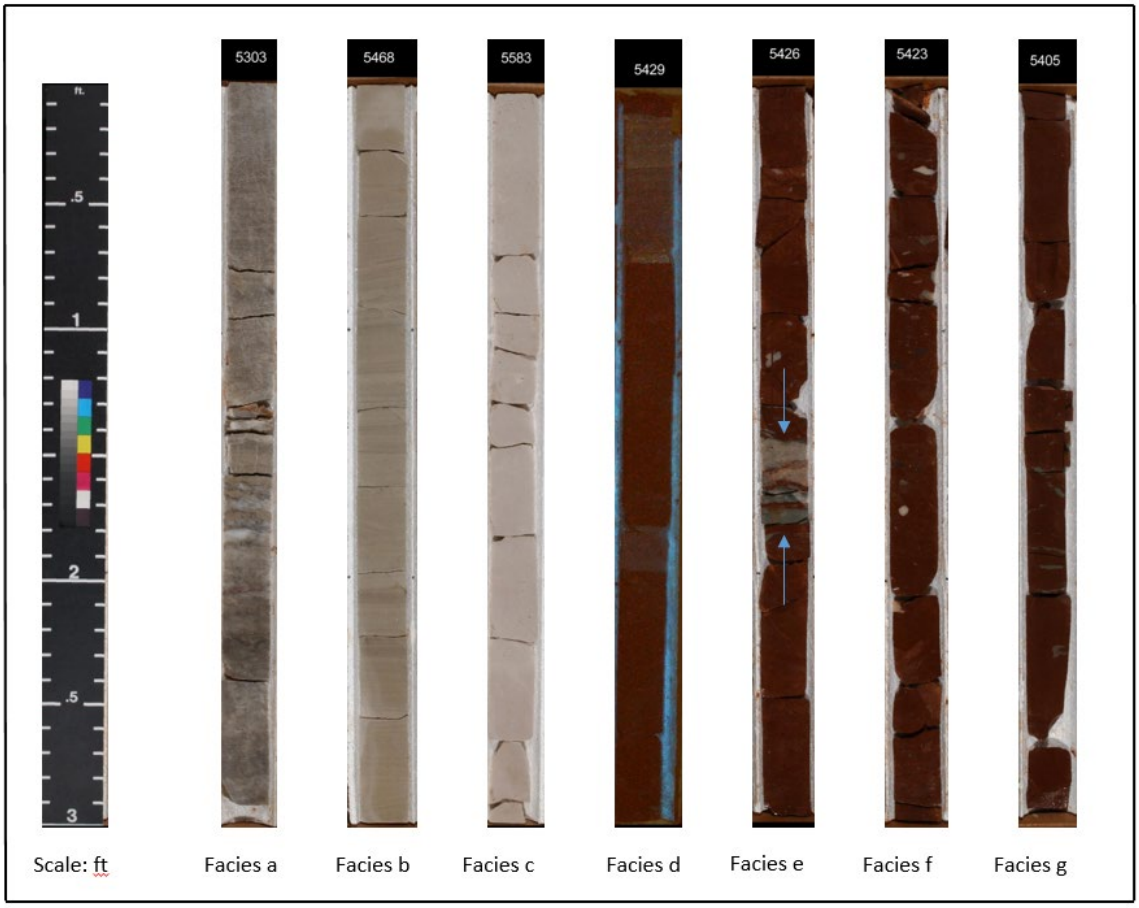

Figure 7. Photographs of the core from well 48x-28; (a) to (g) refer to EF1 to EF7, respectively algorithms (Al Hasan et al., 2023).

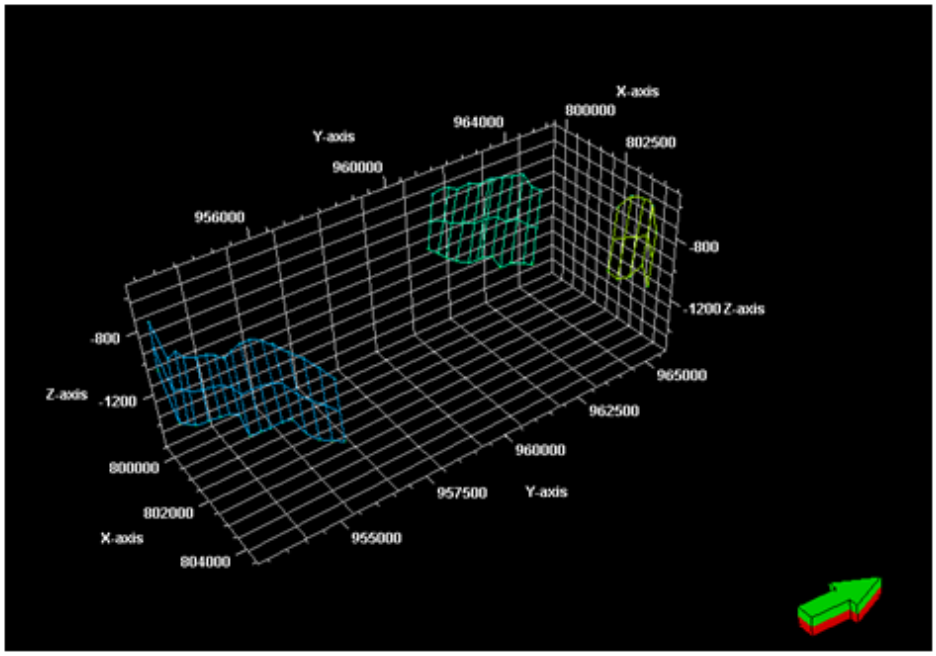

Figure 8. The faults interpreted from seismic sections.

Figure (9-a) shows the Second Wall-Creek Sand and Crow Mountain horizons along with the wells in the field. For the sake of structural modeling, one should

begin by building a base model to assign physical properties (*e.g.*, permeability). In this study, we employed a 50 x 50 grid layout, strategically designed for the horizontal direction, paired with a vertical resolution of 1 meter. This configuration allows us to achieve a high level of granularity, facilitating a more nuanced and accurate representation of the EFs within each individual grid cell. By using this specific grid size and resolution, we can capture subtle variations in the EFs characteristics, ensuring that our analysis reflects the complexities of the subsurface environment more effectively. This approach enhances the reliability of our findings and supports more informed decision-making based on the detailed spatial data we collected. This had to be done considering the state of the fault planes and their effects on the model. Indeed, the presence of faults called for modifications to the primary grids of the model. This was done using the pillar gridding method. To do this, the reservoir area was generally defined and the fault planes were further declared, so that the entire reservoir area could be grided along with the faults (Figure 9-b). As shown in Figure 9-b, the presence of fault planes changes the homogeneity of the grid sizes.

After gridding the model of reservoir and the regional faults, we came up with an initial model (Figure 10-a). On this model, the horizontal and vertical surfaces

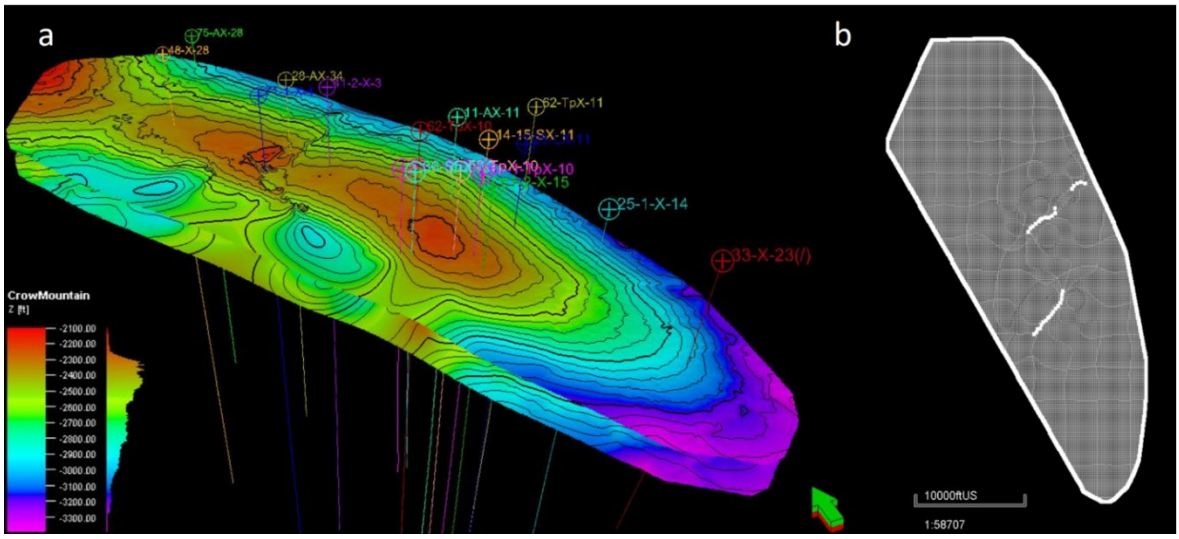

Figure 9. (a) Depth models made for the interval between the Second Wall-Creek Sand and Crow Mountain horizons with some of the wells in the field. (b) The gridded range of the reservoir using pillar gridding, is a mid-skeleton map used to orientate grig according to fault trend.

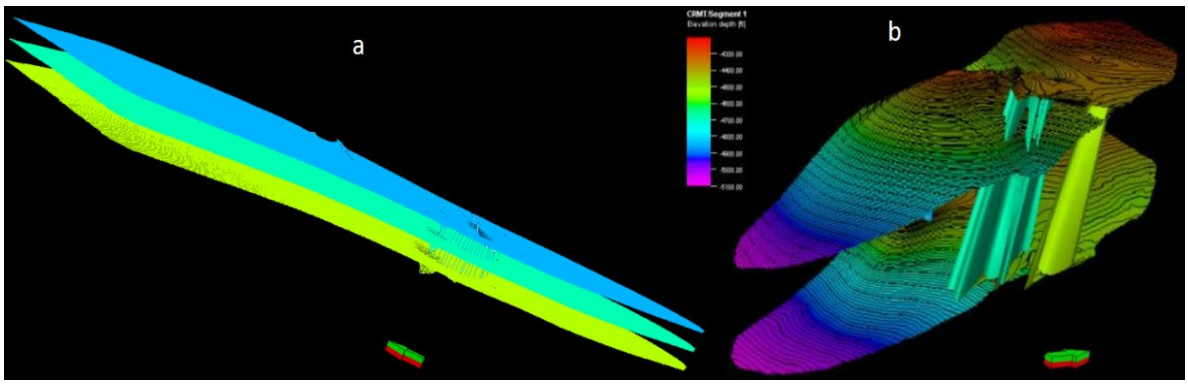

Figure 10. (a) Final gridding of the base model after fault modelling to include faults in the gridding process. (b) The structural model of the interval between the Second Wall-Creek Sand and Crow Mountain horizons.

refer to 3D fault planes in the region. Limited fault modeling was done between the Second Wall-Creek Sand and Crow Mountain reservoir horizons, as shown in Figure 10-b.

6-1 geostatistical modelling of EFs

The 3D EFs model was generated in Petrel. Conceptually, EFs and petrophysical data conditioned by facies simulation (porosity, permeability, and water saturation) are propagated across the entire reservoir from wells, adopting geostatistical methods (Schlumberger, 2008).

A major contribution of geostatistics to reservoir modeling is to address the major problem of data integration, where it can serve as a method for integrating different data, with different scales, into a more accurate numerical reservoir model. Unlike most traditional deterministic methods, geostatistical algorithms indicate the degree of uncertainty of the obtained model. To integrate EFs from well logs with the seismic-derived 3D grid, we employed an upscaling method in Petrel software. We used the 'Most of' method in the Facies Upscaling module, which applies a majority rule to assign each grid cell the most frequent facies from the underlying well log data. This approach is suitable for categorical EFs, ensuring the dominant facies are preserved while aligning with the coarser seismic resolution. The method's efficiency also supports its use for the large Teapot Dome dataset.

The variogram serves to characterize the spatial distribution pattern of the EFs. The dimensions and orientation of the geological formations are closely associated with the selected variogram ranges (Al-Houti et al., 2013). A variogram is characterized by four primary parameters: major direction, minor direction, vertical direction, and azimuth or orientation (Bohling, 2005, Kiaei et al 2015). Table 6 presents the results of the variogram parameters for the EFs between the Second Wall-Creek Sand and Crow Mountain horizons in the studied oil field. This table succinctly highlights the characteristics of the selected variogram across three spatial directions. Notably, the chosen variogram demonstrates a remarkably low nugget effect, which signifies the variogram model's effectiveness. It's critical to note that using models with a high nugget effect can lead to significant errors in simulating EFs and their associated properties. The nugget effect reflects substantial variations in the variable over short distances, indicating variations on a spatial scale smaller than the sample scale or potential inaccuracies in variable measurement. This insight underscores the reliability of our variogram approach in capturing the intricate dynamics of the EFs.

Facies simulation was performed by adopting an appropriate variogram for each EFs within the specified zones (the interval between the Second Wall-Creek Sand and Crow Mountain horizons in this study) using the SIS method. Inputs to facies simulation (SIS) were Log-EFs from MRGC (Figure 11-a) and SOM (Figure 11-b) methods, respectively. On Figure 11, the model is demonstrated laterally from the west.

Table 6. Characteristics of the variograms identified for each zone between the Second Wall-Creek Sand and Crow Mountain horizons.

Sill	Nugget	Vertical Range	Minor Range	Major Range	Model	Zone	
0.9729	0.0858	20.259	2012.021	2063.547	Spherical	Zone1	EFS
0.966	0.0107	22.834	2613.883	4328.887	Spherical	Zone2	
1.000	0.0001	10.156	1586.289	3165.809	Spherical	Zone3	
0.980	0.0001	18.736	2063.919	5756.405	Spherical	Zone4	
0.997	0.0137	23.543	2261.589	3763.727	Spherical	Zone5	
0.9727	0.0001	20.000	2047.250	3572.527	Spherical	Zone6	
0.9727	0.0835	23.285	3281.798	4158.116	Spherical	Zone7	

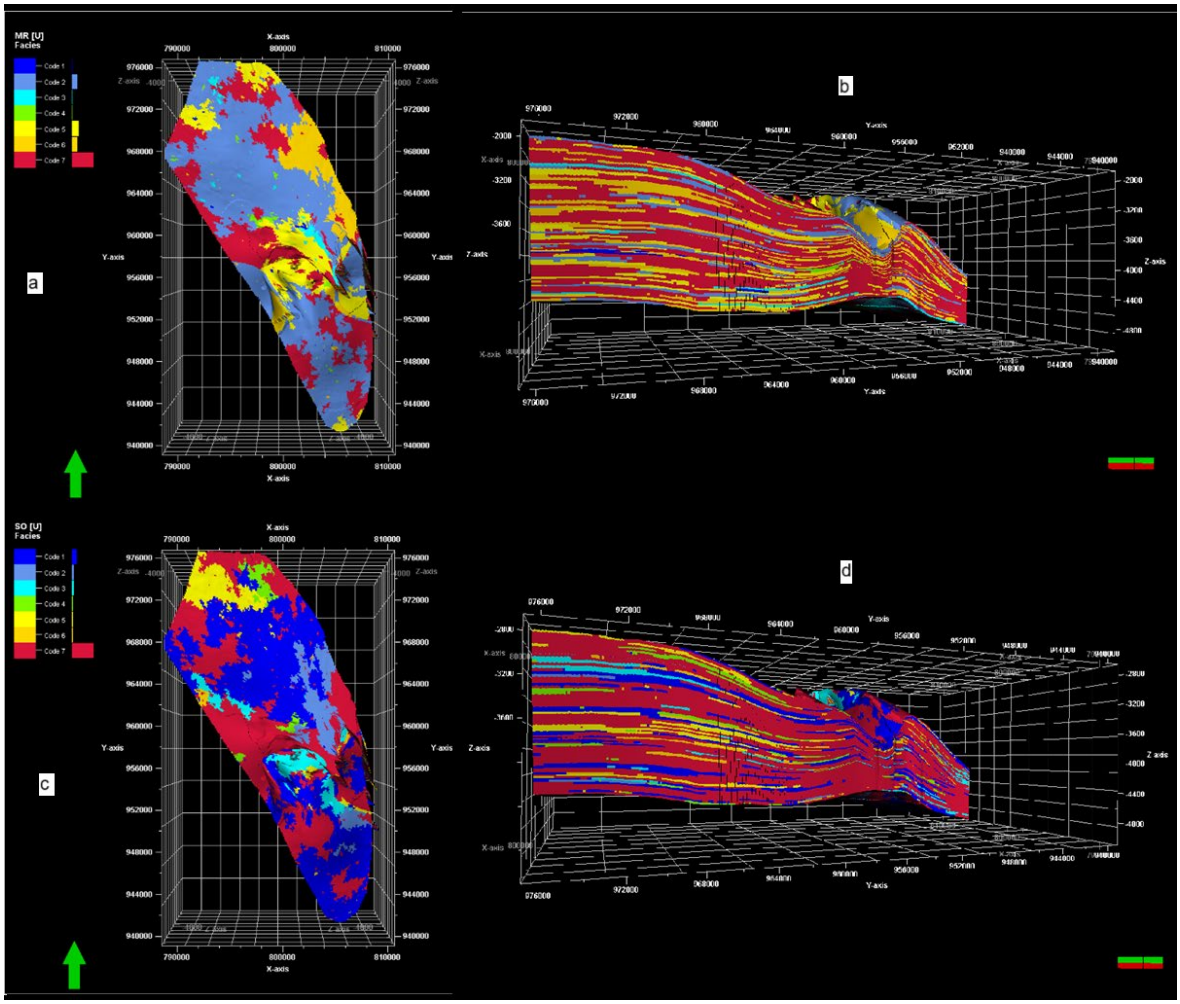

Figure 11. (a,b) MRGC-based and (c,d) SOM-based 3D EFs model and integration of well and seismic interpreted data using the SIS between the second well Creek and Crow Mountain horizons (vertical view on the left and westward view on the right).

The enhanced geological interpretation of the Teapot Dome field (Second Wall Creek Sand to Crow Mountain horizons) links the distribution of high-quality facies to geological processes. The MRGC-based model identifies the best reservoir-quality facies (EF1 and EF2) in the northeastern and southern regions, likely representing proximal deltaic channels and mouth bars with high porosity due to favorable deposition and limited diagenetic cementation. The SOM-based model partially agrees, placing high-quality facies in the middle to northern and southern areas, suggesting transitional deltaic zones. The anticlinal structure and faults at Teapot Dome influenced sediment accumulation and preservation, enhancing reservoir quality in these regions. This interpretation supports drilling new wells in the northeastern and southern parts, where depositional, diagenetic, and structural factors converge, as validated by well 48X-28 log data. Figure 12 shows the intersection of inline 255 from the final model with the EFs log of well 48X-28, which we kept as a blind well.

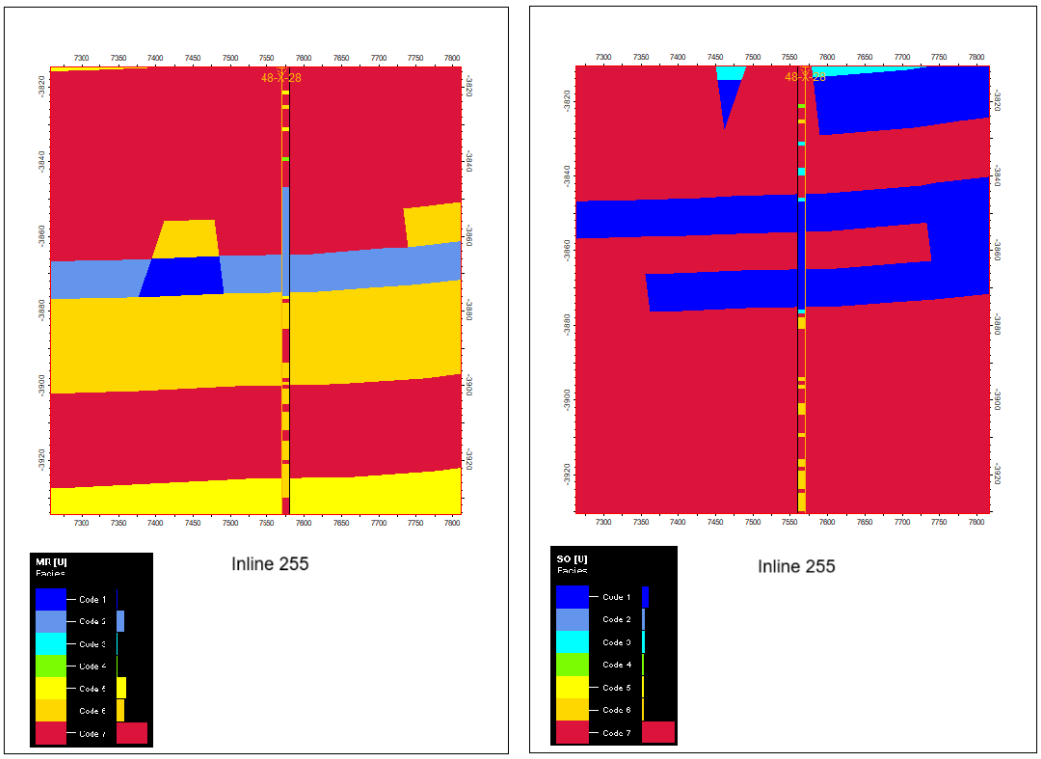

Figure 12. The intersection of inline 255 taken from the final model with the EFs log of well 48X-28 for (a) MRGC and (b) SOM.

6-2 Facies Proportion Validation

To rigorously validate the EFs model based on the MRGC and SOM methodologies, we meticulously compared the EFs ratios derived from these models against those extracted from the original well logs and their enhanced iterations. Figure 13 illustrates the relative distribution of seven distinct EFs across the geological interval from Sand Second Wall Creek to Crow Mountain in the renowned Teapot Dome field. The data is represented with well logs depicted in red, enhanced cells in green, and the outputs of the MRGC and SOM models illustrated in blue.

Among these EFs, EF7 dominates the landscape, representing 54.1% of the model's total, which closely aligns with the enhanced cells at 54.0% and the well logs at 52.0% for the MRGC model. For the SOM model, EF7 accounts for an even larger portion, reflecting 63.7% in comparison to 65.9% for the enhanced cells and 59.9% for the well logs, all validating the model's effectiveness in capturing the reservoir's essential characteristics.

EF1 and EF2, indicative of the highest reservoir quality, also reveal remarkably similar proportions in the results. This close correlation underscores the accuracy of our distribution and modeling processes. The strong agreement between the MRGC and SOM models and the well log data enhances their utility in reservoir characterization. It suggests that a focused data collection strategy in the northeast and southern regions—where EF1 and EF2 are predominantly located—would be a promising approach for further exploration and analysis.

As can be seen from both models, the MRGC model performs better. It is based on a relative density-based algorithm, making it more robust to noisy or heterogeneous data, such as sharp differences in rock properties between wells and missing or incomplete data. This is demonstrated in EF1 and EF2, compared to the same two EFs from SOM and their distribution in the resulting model.

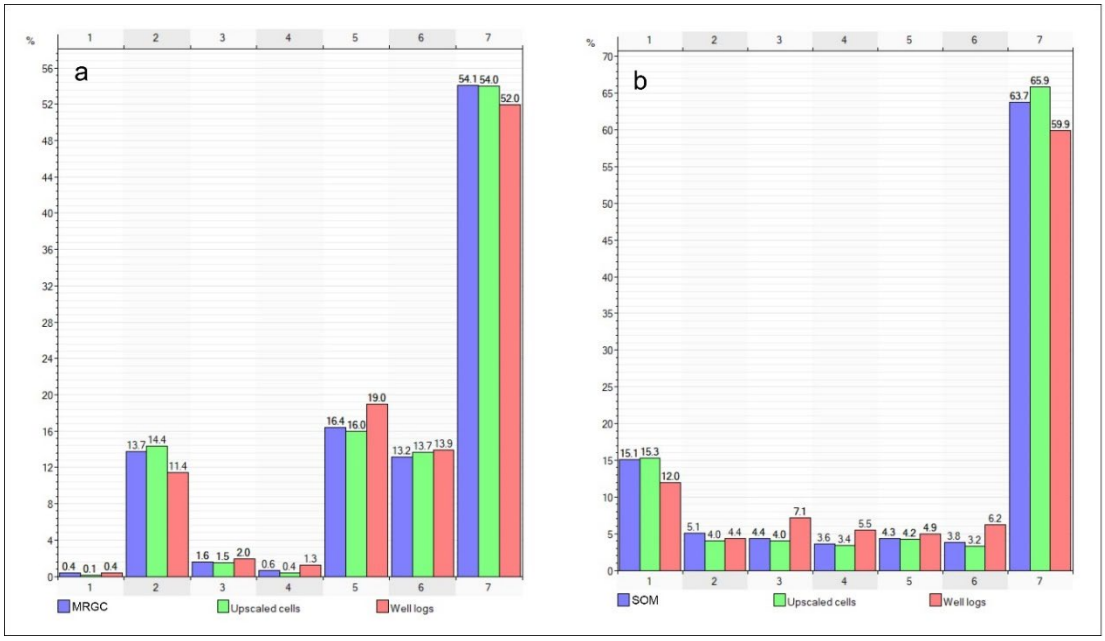

Figure 13. Histogram of EFs for well logs, upscaled cells, and (MRGC, SOM) models.

7 Conclusion

The thorough study of electro–facies (EFs) in the Teapot Dome field from the Second Wall Creek Sand to Crow Mountain horizons shows that both the Self-Organizing Map (SOM) and Multi-Resolution Graph Clustering (MRGC) methods were successful in characterizing the reservoir in this discipline-specific illustrative case study. Using the SOM and MRGC clustering for well 48X-28 with its clustering validated by cross-plots (Figures 3-4) and core photographs (Figure 7) led to recognizing seven EFs; EF1 and EF2 represented at least the highest quality reservoir characterized by lowest gamma ray (GR) and highest sonic transit time (DT, Figure 4a-d), while cross-plotting GR and neutron porosity (NPHI) logs (Figure 5) more specifically described the relationship between EFs and relevant petrophysical properties, confirming comparable depths of high porosity in EF1 and EF2 consistent with proximal deltaic channels and mouth bars.

3D geological models are generated in Petrel using Sequential Indicator Simulation (SIS) with seismic information and well logs to identify facies (EF1 and EF2), which are located in the northeastern and southern parts of the field (see EF1 and EF2 in Figure 12). The MRGC method performed much better than SOM because the MRGC was able to confirm the well log data (Figure 6) more closely and had better facies proportion validation (Figure 13). For example, EF7 comprised 54.1% in the MRGC model and 63.7% in the SOM model, and well logs (52.0%) and upscaled cells (54.0%) are close to each other. The variograms (Table 6) further emphasized the models' validity, which presented acceptable nugget effects and sufficient spatial extent to show that the EFs have sufficient distance separation between them.

The research findings, which are supported by the fault modeling (Figure 8) and structural gridding (Figures 9 and 10) in this study, clearly demonstrate the impact of geological structures on reservoir quality. The clear advantage of the MRGC-based empirical model, especially when considering data variability in heterogeneous data sets, better represents quality zones for informed drilling plans in marginal reservoir quality zones (EF1 and

EF2) in the northeastern and southern areas of this study area. This study advances reservoir characterization through integrated data analysis and geostatistical modeling, delivering actionable insights that improve reservoir management and drilling efficiency. The proposed well locations, grounded in a robust 3D EFs model, pave the way for more effective and economical resource extraction.

References

Abdel-Fattah, M. I., Metwalli, F. I. & El Sayed, I. M. 2018, Static reservoir modeling of the Bahariya reservoirs for the oilfields development in South Umbarka area, Western Desert, Egypt. Journal of African Earth Sciences, 138, 1-13.

Ajil, K. S., Thapliyal, P. K., Shukla, M. V., Pal, P. K., Joshi, P. C. & Navalgund, R. R. 2010, A new technique for temperature and humidity profile retrieval from infraredsounder observations using the adaptive neuro-fuzzy inference system: IEEE Transactions on Geoscience and Remote Sensing, 48(4), 1650−1659.

Al Hasan, R., Saberi, M. H., Riahi, M. A., & Manshad, A. K. 2023, Electro-facies classification based on core and well-log data. Journal of Petroleum Exploration and Production Technology, 13(11), 2197-2215.

Alizadeh, B., Najjar, S., & Kadkhodaie-Ilkhchi, A. 2012, Artificial neural network modeling and cluster analysis for organic facies and burial history estimation using well-log data: A case study of the South Pars Gas Field, Persian Gulf, Iran: Computers & Geosciences, 45(4), 261−269.

Amiri, A., Bagheri, M., & Riahi, M. A. (2020). Simplified automatic seismic to well tying using smooth dynamic time warping technique in R. Iranian Journal of Oil and Gas Science and Technology, 9(4), 85-92.

Ariyan Nezhad, A., Radad, M., & Hadiloo, S. (2020). Unsupervised Seismic Data Classification Using Gaussian Mixture Models. *Journal of Petroleum Research*, *30*(99-3), 129-144.

Asadi Mehmandosti, E., Mirzaee, S., Moallemi, S. A., & Arbab, B. 2017, Study and 3D modeling of the Dariyan Formation Electrofacies by using Geostatistics, in one of the Persian Gulf Oilfields. Kharazmi journal of earth sciences, 3(1), 25-44.

Asante, J. & Kreamer, D. 2015, A new approach to identify recharge areas in the Lower Virgin River Basin and surrounding basins by multivariate statistics: Mathematical Geosciences, 47(7), 819−842.

Asquith, G. B., Krygowski, D. & Gibson, C. R. 2004, Basic well log analysis (Vol. 16). Tulsa: American Association of Petroleum Geologists.

Bagheri, M., & Riahi, M. A. (2013). Support vector machine based facies classification using seismic attributes in an oil field of Iran. Iranian Journal of Oil and Gas Science and Technology, 2(3), 1-10.

Bagheri, M., & Riahi, M. A. (2015). Seismic facies analysis from well logs based on supervised classification scheme with different machine learning techniques. Arabian Journal of Geosciences, 8(9), 7153-7161.

Bagheri, M., & Riahi, M. A. (2017). Modeling the facies of reservoir using seismic data with missing attributes by dissimilarity based classification. Journal of Earth Science, 28, 703-708. https://doi.org/10.1007/s12583-017-0797-6

Bagheri, M., Riahi, M. A., & Hashemi, H. (2013). Reservoir lithofacies analysis using 3D seismic data in dissimilarity space. Journal of Geophysics and Engineering, 10(3), 035006.

Behbehani, S., Hollis, C., Holland, G., Singh, P. & Edwards, K. 2019, A seis-

mically controlled seal breach in a major hydrocarbon province: A study from the Mauddud Formation in the Bahrah field, Kuwait. Marine and Petroleum Geology, 107(July), 255–277. https://doi.org/10.1016/j.marpetgeo.2019.04.017.

Bohling, G., 2005, Stochastic simulation and reservoir modeling workflow. C&PE.

Canet, C., Arana, L., González-Partida, E., Pi, T., Prol- Ledesma, R. M.& Franco, S. I. (2010), A statistics-based method for the short-wave infrared spectral analysis of altered rocks: An example from the Acoculco Caldera, Eastern Trans-Mexican Volcanic Belt: Journal of Geochemical Exploration, 105(1−2), 1−10.

Dennen, K., Burns, W., Burruss, R. & Hatcher, K. 2005, Geochemical Analyses of Oils and Gases, Naval Petroleum Reserve No. 3, Teapot Dome Field, Natrona County, Wyoming. US Geological Survey Open-File Report, 1275, 69. Usgs Open-File Report 2005-1275. BiblioBazaar (2013)

Deutsch, C. V., & Journel, A. G. 1992, Geostatistical software library and user's guide. *New York*, *119*(147), 578.

Deutsch, C.V., & Hewett,T.A. 1996, "Challenges in reservoir forecasting," Mathematical Geology, vol. 28, no. 7, pp. 829–842.

Dolton, G. L., & Fox, J. E. 1995, Powder River Basin Province (033). Gautier, DL, Dolton, GL, Takahashi, KI, and Varnes, KL, eds.

Fiedler, M. 1973, Algebraic connectivity of graphs: Czechoslovak Mathematical Journal, 23(2), 298−305.

Filak, J. M., Van Lint, J., Ali, F., Ma, E., & Al-Houti, R. 2013, Advanced Workflow for 3-D Geological Modeling of a Complex Giant Field, Greater Burgan, Kuwait. In SPE Middle East Oil and Gas Show and Conference (pp. SPE-164294). SPE.

Fukunaga, K., & Hostetler, L. 1975, The estimation of the gradient of a density function, with applications in pattern recognition: IEEE Transactions on Information Theory, 21(1), 32−40.

Gressly, A., 1838, Observations geologiques sur le Jura Soleurois. Neue Denkschr. Allg Schweiz, Ges. Naturw., 2, pp. 1–112.

Hadiloo, S., Radad, M., Mirzaei, S., & Foomezhi, M. (2017, June). Seismic facies analysis by ANFIS and fuzzy clustering methods to extract channel patterns. In 79th EAGE Conference and Exhibition 2017 (Vol. 2017, No. 1, pp. 1-5). European Association of Geoscientists & Engineers.

Hatampour, A., Schaffie, M., & Jafari, S. 2015, Hydraulic flow units, depositional facies and pore type of Kangan and Dalan Formations, South Pars Gas Field, Iran: Journal of Natural Gas Science and Engineering, 23, 171−183.

Iltaf, K. H., Yue, D., Wang, W., Wan, X., Li, S., Wu, S., ... & Tahir, M. 2021, Facies and Petrophysical Modeling of Triassic Chang 6 Tight Sandstone Reservoir, Heshui Oil Field, Ordos Basin, China. Lithosphere, 2021(Special 1), 9230422.

Jafri, M. K., Lashin, A., Ibrahim, E., & Naeem, M. 2016, Petrophysical evaluation of the Tensleep Sandstone formation using well logs and limited core data at Teapot Dome, Powder River Basin, Wyoming, USA. Arabian Journal for Science and Engineering, 41(1), 223-247.

Jahanjooy, S., Hashemi, H., Bagheri, M. et al. Seismic-well tie using fuzzy properties of acoustic impedance in the dynamic time warping. Earth Sci Inform 18, 205 (2025). https://doi.org/10.1007/s12145-025-01697-0

Jain, A. K.; Murty, M. N., &Flynn, P. J. 1999, Data clustering: A review: ACM Computing Surveys, 31(3), 264−323.

Journel, A.G. & Gomez-Hernandez, J.J.,

1993, Stochastic imaging of the Wilmington clastic sequence. SPE formation Evaluation, 8(01): 33-40.

JRL, A. (1976). Selley. R. C. 1976, An Introduction to Sedimentology. xi 408 pp., 162 figs. Academic Press, London. Price £9.90 (cloth); £5.90 (softback). ISBN 0 12 636350 1 (cloth); 0 12 636356 0 (soft). Geological Magazine, 113(5), 491-492. doi:10.1017/S0016756800050834

Kiaei, H., Sharghi, Y., Ilkhchi, A. K., & Naderi, M. 2015, 3D modeling of reservoir electrofacies using integration clustering and geostatistic method in central field of Persian Gulf. Journal of Petroleum Science and Engineering, 135, 152-160.

Kohonen, T., 1990, The SOP: Proceedings of the IEEE, 78(9), 1464−1480.

Ma, Y. Z., & Zhang, X. 2019, Quantitative geosciences: Data analytics, geostatistics, reservoir characterization and modeling (p. 640). Cham: Springer International Publishing.

Macqueen, J. 1967, Some Methods for classification and Analysis of Multivariate Observations, in LeCam, L. M., and Neyman, J., Eds., Proceedings of the 5th Berkeley Symposium on Mathematics Statistic and Probability,Volume 1: Statistics, University of California Press,USA, 281−297.

Mirzakhanian, M., & Hashemi, H. (2022). ANFIS rules driven integrated seismic and petrophysical facies analysis. *Journal of the Earth and Space Physics*, *47*(4).

Omidvar, A., Kamali, M., & Kazemzadeh, E. 2013, Static Three Dimensional Simulation and Estimation of Reservoir Parameters Using Geostatistical Methods in One of Iranian Reservoirs. Journal of Petroleum Research, 23(75), 49-57.

Schlumberger, 2008, Petrel Introduction Course, Seismic-to-Simulation Software Petrel Introduction Course.

Selley, R. C. 1986, Ancient sedimentary and environment and theirsubsurface diagnosis. Chapman and hall, London. 3rd ed. 317 pp.

Teapot Dome 3D Survey. http://wiki.seg.org/wiki/Open_data.

Tian, Y., Xu, H., Zhang, X. Y., Wang, H. J., Guo, T. C., Zhang, L. J., & Gong, X. L. 2016, Multi-resolution graph-based clustering analysis for lithofacies identification from well-log data: Case study of intraplatform bank gas fields, Amu Darya Basin. Applied Geophysics, 13(4), 598-607.

Ward, W. O. C., Wilkinson, P. B., Chambers, J. E., Oxby, L. S., & Bai, L. 2014, Distribution-based fuzzy clustering of electrical resistivity tomography images for interface detection: Geophysical Journal International, 197(1), 310−321.

Webber, K. J., & Van Geuns, L. C. 1990, Framework for constructing clastic reservoir simulation models. Journal of Petroleum Technology, 42(10), 1248-1297.

Ye, S. J., & Rabiller, P. 2000, A new tool for electrofacies analysis: Multi-Resolution Graph Based Clustering: SPWLA 41st Annual Logging Symposium,Dallas, Texas, USA, Jun 4−7.

Zare, A., Bagheri, M., & Ebadi, M. (2020). Reservoir facies and porosity modeling using seismic data and well logs by geostatistical simulation in an oil field. Carbonates and Evaporites, 35(3), 65. https://doi.org/10.1007/s13146-020-00605-5

Zhang T-F, Tilke P, Dupont E, Zhu L-C, Liang L. & Bailey W, 2019, Generating geologically realistic 3D reservoir facies models using deep learning of sedimentary architecture with generative adver- sarial networks. Petroleum Sci 16(3):541–549.